Tuning Crystal Packing and Magnetic Properties in a Series of [Dy 12] Metallocubanes Based on Azobenzene Derivatives of Salicylic Acid

Ivan Khariushin, Alexander Ovsyannikov, Daut Islamov, Aida Samigullina, Svetlana Solovieva, Jakub Zakrzewski, Szymon Chorazy, Sylvie Ferlay

Tuning Crystal packing and Magnetic Properties in a series of [Dy_{12}] Metallocubanes based on Azobenzene derivatives of Salicylic Acid

Ivan V. Khariushin[†], Alexander S. Ovsyannikov[§], Daut R. Islamov[§], Aida I. Samigullina[§], Svetlana E. Solovieva[§], Jakub J. Zakrzewski[‡], Szymon Chorazy[‡] and Sylvie Ferlay[†]*

[†]*Université de Strasbourg, CNRS, CMC UMR 7140, F-67000 Strasbourg, FRANCE*

[§]*Arbuzov Institute of Organic and Physical Chemistry, FRC Kazan Scientific Center, Russian Academy of Sciences, Arbuzova 8, Kazan, 420088, RUSSIAN FEDERATION*

[‡]*Faculty of Chemistry, Jagiellonian University, Gronostajowa 2, 30-387 Krakow, POLAND*

* ferlay@unistra.fr

ABSTRACT

A series of four new Dy_{12} dodecanuclear clusters based on azobenzene derivative ligands of salicylic acid (**L1**-**L4**) has been synthesized and characterized in the crystalline phase using X-ray diffraction on single crystal (SCXRD) and powder (PXRD), IR-spectroscopy, elemental analysis, DSC-TGA method. It was revealed that all obtained clusters exhibit the formation of the similar metallic cluster nodes, as vertex-sharing heterocubanes, obtained from four Dy^{3+}

cations, three bridging hydroxyl groups and O atoms from the salicylic ligands. The coordination geometry around the Dy(III) centers has been carefully analyzed. Whereas **Dy_{12}-L1** and **Dy_{12}-L2** with **L1** and **L2** containing Me and OMe groups in *para* positions of phenyl rings, respectively, form similar porous 3D diamond-like molecular networks due to CH-π interactions, for **Dy_{12}-L3** with **L3** bearing NO_2-electron withdrawing group, the generation of 2D molecular grids assembled by π-π staking is observed, and for **Dy_{12}-L4** with **L4** bearing phenyl substituent, 3D hexagonal channels have been generated. The complexes **Dy_{12}-L1**, **Dy_{12}-L2** and **Dy_{12}-L3** exhibit zero-field slow magnetic relaxation effect. After UV-irradiation of **Dy_{12}-L1**, a decrease of the magnetic anisotropy energy barrier displaying the possibility of control over magnetic properties by external stimulus, has been observed.

INTRODUCTION

In the last decades, lots of efforts have been devoted to the building of new magnetic materials, for which the synergy between magnetism and porosity can lead to compounds like magnetic sensors/sponges or low-density magnets, for example.[1,2,3] Among magnetic materials, one may mention the Single Molecular Magnets (SMMs) – generally characterized by their organic or hybrid organic-inorganic nature and that display slow relaxation of their magnetization, equivalent to a magnetic memory effect.[4] Thus, they may find applications in new high-density information storage, magnetic qubits, spintronic devices. In the last decades, a lot of studies were focused on the preparation of SMMs based on cluster complexes involving d-, f- and both d- and f- cations.[5] Among them, it was shown that lanthanide based molecular systems exhibit the best values of blocking barriers due to high intrinsic magnetic anisotropy of lanthanide ions.[6] However, recent studies show that the

magnetic behavior of 4f-SMMs is very dependent on many parameters such as molecular structural environment, ligand field effects, presence of electron donating or withdrawing chemical groups, and the distances between the cluster centers within the crystal packing, that all may significantly affect the intra- and intermolecular magnetic interactions.[7]

In the last decades, high nuclearity lanthanides clusters have attracted great interest, due to their intriguing physical properties,[8] in optics and magnetism, as Single Molecular Magnets[5] or compounds presenting MagnetoCaloric Effects (MCEs).[9] The observed cluster nuclearity can reach values up to 104, for Keplerate derivatives.[10] The high-nuclearity homometallic Ln_{12} compounds have been discovered two decades ago. Different types of geometries have been displayed by the Ln_{12} metallic clusters. The first reported compound, with the core $[Ln_{12}(\mu_3\text{-}OH)_{16}(I)_2]^{18+}$ (Ln = Dy and Er) fused by tyrosine ligands, where the core is a four-vertex sharing heterocubane-like, with a I- on each side of the square plane (type **A**, Figure 1).[11] An analogous arrangement was found recently for the compounds of formula $[Ln_{12}(fsa)_{12}(\mu 3\text{-}OH)_{12}(DMF)_{12}]\cdot nDMF$ (Ln = Eu, Gd, Dy), obtained from salicyclic acid (H_2fsa).[12] The Dy derivative show a SMM (Single Molecule Magnet) behavior, while the Gd derivative presents a large magnetocaloric effect. A compound of formula $\{Dy_{12}(OH)_{16}(phenda)_8(H_2O)_8\}^{4+}](X)$ was reported (phenda = 1,10-phenanthroline-2,9-dicarboxylic acid) showing also a type **A** arrangement and exhibiting slow magnetic relaxation.[13] Using salicylic derivatives another dodecanuclear complex was obtained, where Ln_{12} wheels containing six vertex-sharing Ln_3 triangle motifs staggered in a crown shape was firstly described for $([Ln_{12}(L)_6(OH)_4O_2(CO_3)_6][Ln_{12}(L)_6(OH)_4O_4(CO_3)_6]\cdot\text{-}\ (ClO_4)_4\cdot xH_2O)$ (L = deprotonated N1,N3-bis(3- methoxysalicylidene)diethylenetriamine and Ln = Dy or Ho)

(type **B**, Figure 1).[14] The presence of carbonate anions induces the formation of these high nuclearity clusters.

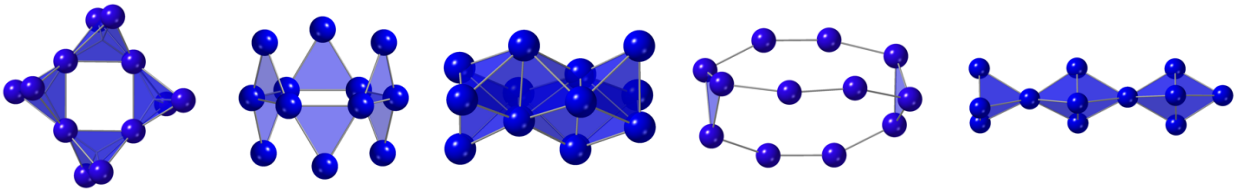

Type **A** Ref 11, 12, 13 | Type **B** Ref 14 | Type **C** Ref 15 | Type **D** Ref 16 | Type **E** Ref 17

Figure 1: The different types of Ln_{12} arrangements in clusters, reported in the literature

A Nd_{12} O/Se bridged units of formula $[(py)_{18}Nd_{12}O_6Se_4(Se_2)_4(SePh)_4(Se_2Ph)_2Hg_2(SePh)_4][(Hg(SePh)_3]_2$ has also been reported where the metallic ions are stacked in four sets of Nd_3, with pairs of tetrahedral oxo ligands separating the Nd_3 planes (type **C**, Figure 1).[15] The same organization for the metallic species has been observed. For the compounds of formula $[Ln^{III}_{12}Na_3(\mu_3\text{-}OH)_2(hmmp)_6(piv)_{12}(CO_3)_6(MeOH)_6]OH{\cdot}5MeOH$ {Ln = Gd , Dy ; hmmpH2 = 2-[(2-hydroxyethylimino)- methyl]-6-methoxyphenol, presenting interesting Cryogenic Magnetocaloric Effect for Gd_{12} compounds, and also SMM for Dy_{12} compounds (type **D**, Figure 1).[16]

Using another approach, the formation of another dodecanuclear lanthanide-based complex was reported $[Dy_{12}(1\text{-}3H)_3(1\text{-}2H)_3(PhCO_2)_5(OH)_{16}\text{-}(H_2O)_{21}]$ (1-nH is a tetrazole decorated calixarene derivative) (type **E**, Figure 1).[17] In this case, the building of the dodecanuclear unit is slightly different and result from apex-fused Ln_5O_6 trigonal bipyramids, leading to ranges of metallic atoms surrounded by an organic layer. More recently, using a "nanocalix" ligand, a Ln_{12} complex with formula $[Ln_{12}(H_2ovih)_3(\mu_3\text{-}O)_9(H_2O)_{24}(NO_3)_9]{\cdot}2C_6H_{15}N{\cdot}xC_2H_3N{\cdot}9H_2O$

(Ln = Gd (1, x = 3), Tb (2, x = 4), and Dy (3, x = 3) and H_5ovih = N,N'-bis(o-vanillidene)- 1H-imidazole-4,5-dicarbohydrazide (H_5ovih))[18], the construction of the dodecanuclear unit resulting three symmetric {Ln_4} units linked via the via the H_2ovih V-type ligands, with a calix shape. These examples illustrate the richness of shapes observed for the Ln_{12} compounds, that depend on the nature of the ligands used.

Despite a huge number of reports encountered in the literature, devoted to the synthesis and magnetic properties investigation of lanthanide clusters, the role of the nature of the ligand on the self-assembly and influence on the magnetic properties of Single-Molecule Magnets in the crystalline phase is still scarcely described. The rational design of appropriate polydentate ligands bearing well adapted coordination site from the geometrical and electronic points of view for the stabilization of magnetically active 4f-clusters is always attracting much attention. In particular, ligands with photoswitchable azobenzene groups which are widely used for the obtaining of photoresponsive materials,[19] may be of interest for the control of the electronic density around the metallic clusters. The presence of azobenzene groups within the structure of organic ligands involved in the coordination with d- and f- cations afforded a number of discrete molecular complexes[20], some of which based on 3d metallic cations (Mn_{12}[21,22,23] or Fe_4 clusters[24] or Ln-complexes[25]) have been carefully investigated in order to study their magnetic properties or catalytic activities.

Herein, using ligands **L1**-**L4** (Figure 2) bearing salicylic coordinating groups anchored to the azobenzene moieties, we report on the synthesis structural and magnetic properties of a new family of dodecanuclear metallocubane Dy_{12} (clusters adopting type **A**) able to exhibit SMM behavior. Different types of withdrawing or donating groups (Me (**L1**), OMe (**L2**), NO_2

(**L3**) and H (**L4**)) have been appended to the azobenzene moieties, in order to reveal their influence on the magnetic properties and propensity of Dy_{12} clusters to form supramolecular networks resulting from the weak intermolecular interactions in the crystalline phase.

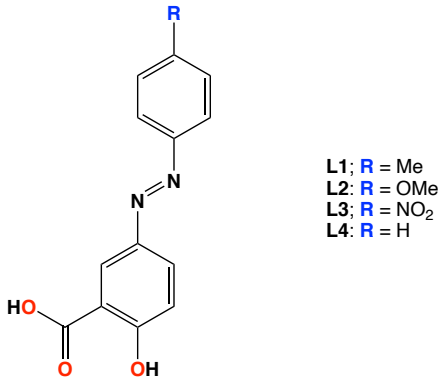

Figure 2: Ligands **L1**, **L2**, **L3** and **L4** used for the formation of new Dy_{12} clusters

EXPERIMENTAL DETAILS

Synthesis

All reagents (including corresponding aromatic amines, salicylic acid, sodium nitrite) were purchased from commercial sources and used without further purification.

^{1}H- and ^{13}C NMR spectra were recorded at 298 K on either Bruker AV400 or Bruker AV500 spectrometers in deuterated solvents, and the residual solvent peak was used as the internal reference. All the chemical shifts (δ) and J values are given in parts per million (ppm) and in Hertz (Hz).

General procedure

The general synthesis for **L1**-**L4** is adapted from an already reported procedure, and is reported below.[33]

Aromatic amine (7.20 mmol) was dissolved in 20 ml of 18% HCl solution. Solution of sodium nitrite (7.20 mmol) in 10 ml of water was added dropwise to aromatic amine solution at 0-5 ^{o}C. The reaction mixture was stirred for 30 minutes at 0-5 ^{o}C. The obtained solution then was added to salicylic acid (7.20 mmol) in 30 ml of saturated sodium carbonate solution. The mixture was stirred for 1 hour at 0-5 ^{o}C and then 2 hours at room temperature. The mixture was neutralized using HCl solution until pH = 6-7 was reached. The azobenzene derivatives were isolated as orange or red precipitate via filtration and washed with large amount of water.

L1

2-hydroxy-5-(p-tolyldiazenyl)benzoic acid. Yield = 60%. Brown solid.

^{1}H NMR (400 MHz, DMSO-d_6) δ (ppm): 8.23 (d, J = 2.69 Hz, 1H), 7.76 (dd, J = 8.07, 2.69 Hz, 1H), 7.70 (d, J = 8.26 Hz, 2H), 7.33 (d, J = 8.07 Hz, 2H), 6.74 (d, J = 8.26 Hz, 1H), 2.38 (s, 3H).

^{13}C NMR (126 MHz, DMSO-d_6) δ (ppm):170.59, 168.81, 150.35, 142.23, 139.71, 129.77, 126.51, 125.49, 121.87, 119.42, 117.54, 20.95

MS (ESI) m/z = 254.9 [M-H]. Anal. Calcd. m/z = 256.08 (see figure S3, SI).

Formula: $C_{14}H_{12}O_3N_2$, Anal. Calcd.: C, 65.62%; H, 4.72%; N, 10.93%; Found: C, 61.28%; H, 5.17%; N, 10.16%

L2

2-hydroxy-5-((4-methoxyphenyl)diazenyl)benzoic acid. Yield = 71%. Brown-orange solid.

^{1}H NMR (400 MHz, DMSO-d6) δ (ppm): 8.29 (d, J = 2.53 Hz, 1H), 8.04 (dd, J = 8.88, 2.53 Hz, 1H), 7.88 (m, 2H), 7.14 (m, 3H), 3.87 (s, 3H).

^{13}C NMR (500 MHz, DMSO-d6) δ (ppm):172.40, 164.05, 162.70, 147.02, 145.48, 129.73, 126.03, 125.29, 119.24, 115.57, 114.66, 56.61.

MS (ESI) m/z = 270.91 [M-H]. Anal. Calcd. m/z = 272.08 (see figure S6)

Formula: $C_{14}H_{12}O_4N_2$, Anal. Calcd.: C, 61.76%; H, 4.44%; N, 10.29%; Found: C, 61.82%; H, 4.48%; N, 10.23%.

L3

2-hydroxy-5-((4-nitrophenyl)diazenyl)benzoic acid. Yield = 65%. Orange solid.

^{1}H NMR (400 MHz, DMSO-d_6) δ (ppm): 8.41 (d, J = 8.90 Hz, 1H), 8.40 (d, J = 2.38 Hz 2H), 8.14 (dd, J = 8.86, 2.38, Hz, 1H), 8.05 (d, J = 8,86 Hz, 2H), 7.19 (d, J = 8.90 Hz, 1H).

^{13}C NMR (500 MHz, DMSO-d_6) δ (ppm): 171.11, 164.74, 155.18, 148.17, 144.47, 129.24, 126.92, 125.09, 123.31, 118.71, 114.14.

MS (ESI) m/z = 285.91 [M-H]. Anal. Calcd. m/z = 287.05 (see figure S9).

Formula: $C_{13}H_9O_5N_3$, Anal. Calcd.: C, 54.36%; H, 3.16%; N, 14.63%; Found: C, 54.32%; H, 3.13%; N, 14.58%.

L4

2-hydroxy-5-((phenyl)diazenyl)benzoic acid. Yield = 64%. Orange solid.

^{1}H NMR (400 MHz, DMSO-d_6) δ (ppm): 8.35 (d, J = 2.5 Hz, 1H), 8.10 (dd, J = 8.9, 2.5 Hz, 1H), 7.89-7.87 (m, 2H), 7.61-7.53 (m, 3H), 7. 17 (d, J = 8.9 Hz, 1H).

^{13}C NMR (500 MHz, DMSO-d_6) δ (ppm): 172.30, 164.62, 152.82, 145.41, 131.11, 130,42, 129.91, 126.68, 123,35, 119,37, 114.79

MS (ESI) m/z = 243.08 [M+H]. Anal. Calcd. m/z = 242.07 (see figure S12).

Formula: $C_{13}H_{10}O_3N_2$, Anal. Calcd.: C, 64.46%; H, 4.16 %; N, 11.56 %; Found: C, 64.39 %; H, 4.17%; N, 11.51%.

Crystallization conditions for Dy_{12}-Ln (n=1-4) clusters

Dy_{12}-L1: 2-hydroxy-5-(p-tolyldiazenyl)benzoic acid **L1** (0.20 mmol) and dysprosium nitrate pentahydrate (0.40 mmol) were dissolved in 18 ml of DMF:EtOH mixture (1:1). The mixture was

stirred for 30 minutes at room temperature. Triethyl amine (1.00 mmol) was added. The mixture was stirred for 24 hours at room temperature and then filtered off. Vapor diffusion during 1 week with acetonitrile caused formation of crystals from filtrate that are suitable for further analysis.

Yield, 43 mg (52%).

Formula: $C_{204}H_{192}Dy_{12}N_{36}O_{60,}$ $2(C_3H_7NO)$ $(C_{168}H_{120}O_{48}N_{24}Dy_{12}\cdot 14DMF)$, Anal. Calcd.: C, 40.58%; H, 3.53%; N, 8.56%; Found: C, 40.1%; H, 3.25 %; N, 8.05 %.

IR (figure S19): 3553 (b), 2929(m), 1652 (s), 1648(s), 1603 (s), 1570 (m), 1487 (s), 1463 (m), 1333 (s), 1274 (m), 1229 (w),1172 (s), 1129 (m), 1074 (w), 929 (w), 891 (w), 839 (s), 771 (m), 738 (w), 681 (m), 623 (m), 606 (w), 571 (m), 523 (w), 479 (m); cm^{-1}

Dy_{12}-L2: 2-hydroxy-5-((4-methoxyphenyl)diazenyl)benzoic acid **L2** (0.18 mmol) and dysprosium nitrate pentahydrate (0.18 mmol) were dissolved in 18 ml of DMF: EtOH mixture (1:1). The mixture was stirring for 30 minutes at room temperature. Triethyl amine (1.00 mmol) was added. The mixture was stirring for 24 hours at room temperature and then filtered off. Vapor diffusion during 1 week with acetonitrile afforded crystals from filtrate that are suitable for further analysis.

Yield, 27 mg (34%).

Formula: $C_{192}H_{210}Dy_{12}N_{32}O_{72}$, $2(C_3H_7NO)$ $(C_{168}H_{120}O_{60}N_{24}Dy_{12}\cdot 10DMF\cdot 4H_2O)$, Anal. Calcd.: C, 38.43%; H, 3.23%; N, 7.70%; Found: C, 39.15 %; H, 3.45%; N, 8.42 %.

IR (figure S19): 3451 (m, b), 2932 (w), 1648 (s), 1597 (s), 1481 (s), 1454 (w), 1428 (m), 1405 (w), 1337 (m), 1249 (s), 1132 (w), 1105 (w) 1028 (w), 839 (m), 770 (m), 720 (w), 683 (w), 622 (w), 573 (w), 504 (w), 437 (w); cm^{-1}

Dy_{12}-L3: 2-hydroxy-5-((4-nitrophenyl)diazenyl)benzoic acid **L3** (0.17 mmol) and dysprosium nitrate pentahydrate (0.17 mmol) were dissolved in 18 ml of DMF: EtOH mixture (1:1). The mixture was stirring for 30 minutes at room temperature. Triethyl amine (1.00 mmol) was added. The mixture was stirring for 24 hours at room temperature and then filtered off. Vapor diffusion during 1 week with diethyl ether afforded crystals from filtrate that are suitable for further analysis.

Yield, 57 mg (73%).

Formula: $C_{192}H_{180}Dy_{12}N_{48}O_{84}$, $10(C_3H_7NO)$ $2(H_2O)$ ($C_{156}H_{84}O_{72}N_{36}Dy_{12}\cdot 22DMF\cdot 2H_2O$), Anal. Calcd.: C, 36.99%; H, 3.88%; N, 11.27%; Found: C, 33.85 %; H, 2.94%; N, 10.53 %.

IR (figure S19): 3455 (w,b), 2931 (w), 1648 (m), 1601 (s), 1553 (w), 1517 (m), 1489 (s), 1467 (w), 1420 (m), 1394 (m), 1335 (s), 1293 (w), 1255 (w), 1220 (w), 1169 (m), 1145 (m), 1105 (m), 1075 (w), 942 (w), 853 (m), 828 (w), 756 (w), 712 (w), 607 (w), 575 (w); cm^{-1}

Dy_{12}-L4: 2-hydroxy-5-((phenyl)diazenyl)benzoic acid **L4** (0.17 mmol) and dysprosium nitrate pentahydrate (0.17 mmol) were dissolved in 18 ml of DMF: EtOH mixture (1:1). The mixture was stirred for 30 minutes at room temperature. Triethyl amine (1.00 mmol) was added. The mixture was stirred for 24 hours at room temperature and then filtered off. Vapor diffusion of solution during 1 week with diethyl ether caused formation of crystals from filtrate that are suitable for further analysis.

Yield, 48 mg (57%).

Formula: $C_{177}H_{167}Dy_{12}N_{31}O_{60}$, $2(C_3H_7NO)$ ($C_{156}H_{86}O_{48}N_{24}Dy_{12}\cdot 9DMF\cdot 5H_2O$), Anal. Calcd.: C, 38.14%; H, 2.78%; N, 8.02%; Found: C, 38.21%; H, 2.82%; N, 7.99 %.

IR (figure S19): 3553(w,b), 2928(w,b), 1669(w), 1654(m), 1593(s), 1568(m), 1560(m), 1478(s), 1439(m), 1406(m), 1385(m), 1326(s), 1306(m), 1274(m), 1250(m), 1207(w), 1169(s), 1135(m),

1122(w), 1077(w), 1019(w), 934(w), 887(w), 843(m), 833(s), 804(m), 757(w), 721(w), 688(s), 653(m), 605(w), 574(m), 517(s), 497(m), 467(m), 442(m), 419(s).

Characterization techniques

X-Ray Crystallography

Diffraction data for single crystals of **Dy_{12}-L1** were collected on Rigaku XtaLab Synergy S instrument with a HyPix detector and a PhotonJet microfocus X-ray tube using Cu-Kα (1.54184 Å). radiation at 100 K. The reflections were indexed and integrated according to the diffraction patterns using the CrysAlisPro data reduction package. Data were corrected for systematic errors and absorption using the ABSPACK module. The GRAL module was used for analysis of systematic absences and space group determination. Using the Olex 2 software,[26] structure was solved by direct methods with SHELXT[27] and refined by the full-matrix least-squares on F2 using SHELXL.[28].

Diffraction data for single-crystals of **Dy_{12}-L2**, **Dy_{12}-L3** and **Dy_{12}-L4** were collected at 100 K on the 'Belok/XSA' beamline (λ = 0.745 Å, 0.7927 Å and 0.80246 Å for **Dy_{12}-L2**, **Dy_{12}-L3** and **Dy_{12}-L4**, respectively, φ-scans) of the Kurchatov Synchrotron Radiation Source (Moscow, Russian Federation).[29,30] Diffraction patterns were collected using Mardtb goniometer equipped with Rayonix SX165 2D positional sensitive CCD detector at 100 K. In total, 300 frames were collected with oscillation range of 1°. The data were indexed, integrated and scaled; absorption correction was applied using the XDS program package.[31] The structures were solved by direct methods with software SHELXT.[27] The structural model was investigated and refined by using Olex 2 software[26] by a full-matrix least-squares method on F2 with anisotropic displacement. All hydrogen atoms were placed in calculated positions and included in the refinement within the

riding model with fixed isotropic displacement parameters Uiso(H) = 1.5Ueq(O), 1.2Ueq(N), and 1.2Ueq(C). The quality of the crystals **Dy_{12}-L1**, **Dy_{12}-L2, Dy_{12}-L3** and **Dy_{12}-L4** necessitated moderate modelling using a range of restraints and constraints to account for the geometric and thermal parameters within parts of the structure, especially when refining the positions of azoaryl substituents.[32] The 0.5/0.5 disordered model was applied for refinement of azoaryl fragments in **Dy_{12}-L1**, **Dy_{12}-L2** and **Dy_{12}-L4**. The hydrogen atoms of coordinated water molecules for **Dy_{12}-L4** were not taken into account in the final refinement, since it is not possible to reliably determine their direction. All disordered solvent molecules located in the interstices between the complexes were not refined, and Solvent Mask command generated by the BYPASS module within Olex2[26] was applied to calculate 1000, 9066, 650 and 4326 electrons per unit cell within solvent accessible voids of 3285 $Å^3$, 17481 $Å^3$, 1204 $Å^3$ and 22092 $Å^3$ for **Dy_{12}-L1**, **D_{12}y-L2**, **Dy_{12}-L3** and **Dy_{12}-L4**, respectively. For **Dy_{12}-L3**, the recovered number of electrons is consistent with 16 DMF, whereas for **Dy_{12}-L1**, **Dy_{12}-L2** and **Dy_{12}-L4** since the large cavities the unidentifiable number and composition of solvate molecules comprising DMF, MeOH, H_2O can present.

The crystallographic data are available for free of charge downloading from the Cambridge Crystallographic Data Centre via www.ccdc.cam.ac.uk/datarequest/cif. CCDC Numbers: 2239122 (**Dy_{12}-L1**); 2239123 (**Dy_{12}-L2**); 2226744 (**Dy_{12}-L3**) and 2239124 (**Dy_{12}-L4**).

Powder diffraction studies (PXRD)

Diagrams were collected on a Bruker D8 diffractometer using monochromatic Cu-Kα radiation with a scanning range between 4 and 40° using a scan step size of 8° mn^{-1}.

IR

The IR spectra of the polycrystalline samples were recorded on a Bruker Tensor 27 spectrometer (Bruker Optic GmbH, Germany) in KBr pellets.

TGA/DSC studies

Thermal stability was studied using a STA 449C Jupiter synchronous microthermoanalyzer (Netzsch, Germany) at heating rate of 10° min^{-1} under argon atmosphere.

Elemental Analysis

Elemental analysis was performed by the Analysis Service of the Faculty of Chemistry of the University of Strasbourg.

Magnetic properties

Magnetic properties were investigated by using a Quantum Design MPMS-3 Evercool magnetometer on the powder samples dispersed in paraffin oil to avoid the rotation of the crystals under an magnetic field. Magnetic data were corrected for the diamagnetic contributions from the sample, oil and the sample holder. Irradiation of samples was performed on the air for powdered microcrystals placed between two 1 mm quartz plates using 365 nm UV flashlight (10 W). The kinetics of light-induced process was not studied, therefore, irradiation was performed overnight (ca. 12 h) to ensure high yield of photoconversion.

RESULTS AND DISCUSSION

Synthesis of the ligands L1-L4

The synthesis of the azo ligands **L1**-**L4** has been briefly described earlier,[33] and to the best of our knowledge, their coordination abilities have not been reported. Till now, one example

involving photoswitchable ligands presenting a salicylic acid derivative and lanthanide cations have been reported, leading to dinuclear species, for which the magnetic properties have not been reported.[34]

The ligands **L1**-**L4** have been obtained in good yields (60% for **L1**, 75% for **L2**, 65% for **L3** and 64% for **L4**) using classical azo C-coupling reaction between a salicylic acid and the appropriate diazonium salt prepared *in situ*, as shown in scheme 1 (see SI).

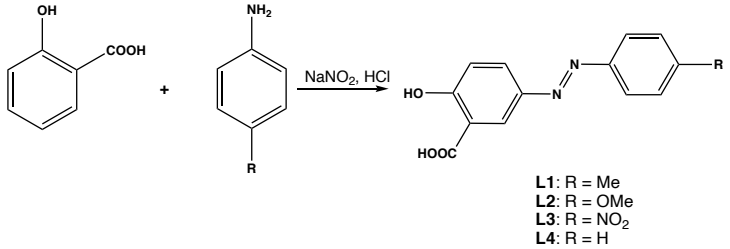

Scheme 1

The ligands have been characterized in solution and in the solid phase (see SI, Figures S1-S12).

Structural description of the {Dy_{12}}-clusters

Single crystals of dysprosium (III) complexes with **L1**-**L4** suitable for X ray diffraction have been obtained using slow evaporation or vapor diffusion techniques involving **L1**-**L4**, $Dy(NO_3)_3$. 6 H_2O mixed with triethylamine in a DMF/MeOH mixture (see a picture of the crystals in SI, Figure S13).

Single crystal X-ray diffraction analysis revealed the generation of four high nuclear coordination compounds of formulas $[Dy_{12}(OH)_{12}(C_{14}H_8N_2O_3)_{12}(C_3H_7NO)_{12})]$ $2(C_3H_7NO)$ (**Dy_{12}-L1**), $[Dy_{12}(OH)_{12}(C_{14}H_{10}N_2O_4)_{12}(C_3H_7NO)_7(OH_2)_5]$ 2 (C_3H_7NO) (**Dy_{12}-L2**), $[Dy_{12}(OH)_{12}(C_{13}H_7N_3O_5)_{12}(C_3H_7NO)_{12}]$ $10(C_3H_7NO)$ $2(H_2O)$ **(Dy_{12}-L3**) and $[Dy_{12}(OH)_{12}(C_{13}H_8N_2O_3)_{12}(OH_2)_4(C_3H_7NO)_{12}]$ $2(C_3H_7NO)$ (**Dy_{12}-L4**) exhibiting the formation

of reproducible neutral {Dy_{12}} metallic cluster core (see SI, crystallographic Table S1). For all the presented compounds, not all solvent molecules have been refined.

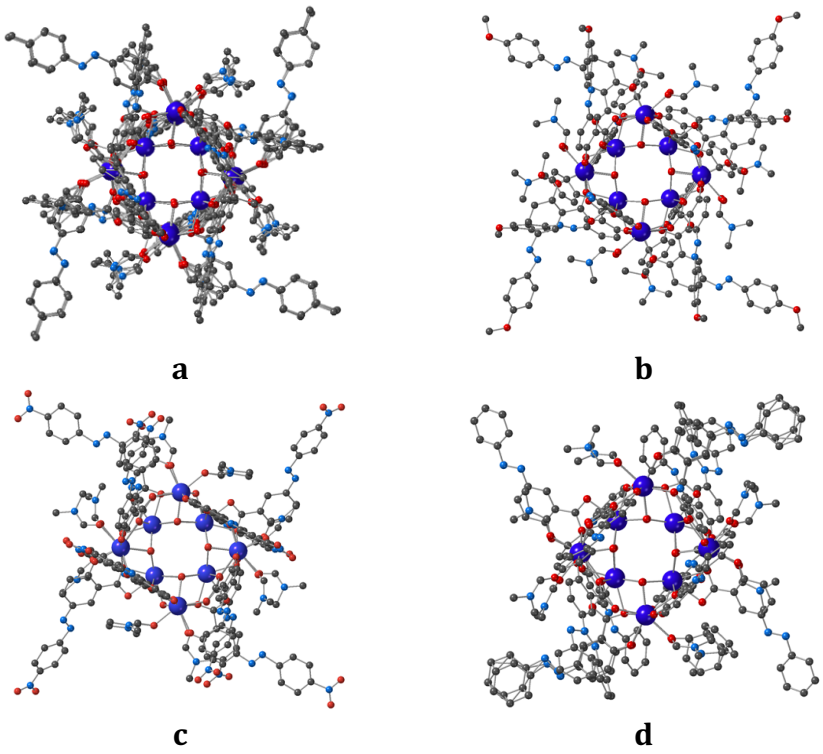

Figure 3. Top view of **Dy_{12}-L1** (a), **Dy_{12}-L2** (b), **Dy_{12}-L3** (c) and **Dy_{12}-L4** (d) clusters. H-atoms and non-coordinated solvent molecules are omitted for clarity. H atoms and non-coordinated solvent molecules are omitted for clarity.

Dy_{12}-L1 and **Dy_{12}-L2** crystallize in the tetragonal $I4_1/a$ space group, **Dy_{12}-L3**, in the triclinic *P*-1 space group, whereas the trigonal *R*-3 space group is observed for **Dy_{12}-L4**. The asymmetric units for the four compounds are presented in Figure S14, with the thermal ellipsoids view with 50% probability. For **Dy_{12}-L1**, the asymmetric unit is composed of three crystallographically independent Dy^{3+} cations, three doubly deprotonated salicylic ligands, three μ_3-OH^- bridging anions and three coordinated DMF molecules. In the case of **Dy_{12}-L2** the similar asymmetric unit is observed, but one coordinated DMF molecules is replaced by a water molecule. For **Dy_{12}-L3** and **Dy_{12}-L4**, the asymmetric unit is composed of six

crystallographically independent Dy^{3+} cations, six doubly deprotonated ligands, six μ_3-OH^- bridging anions and six coordinated DMF/H_2O molecules. All complexes excepting **Dy_{12}-L3** present highly disordered azoaryl moieties, as shown in Figure 3, and contain large pores filled by solvent molecules (see experimental part).

All obtained neutral compounds are based on the formation of dodeconuclear cluster core composed of four fused tetrahedrons formed by Dy atoms and surrounded by 12 doubly deprotonated salicylic ligands, bridged by four hydroxyl groups. Four coordinated salicylic ligands located at the upper and bottom sides of cluster unit form a calix-like shape hydrophobic cavity with approximal size of 4.4 Å, and as shown in Figure 4 a and b, displaying a practically parallel or tilted orientation of opposite salicylic aryl rings (for dihedral angles, see table S2) and accommodating one DMF solvate molecules *via* O-H…O and CH/π interactions (for common distances, see Tables S3-S6). The four lateral positions of the cluster core each are occupied by the four remained salicylic moieties and interacting with solvent molecules (DMF or H_2O)

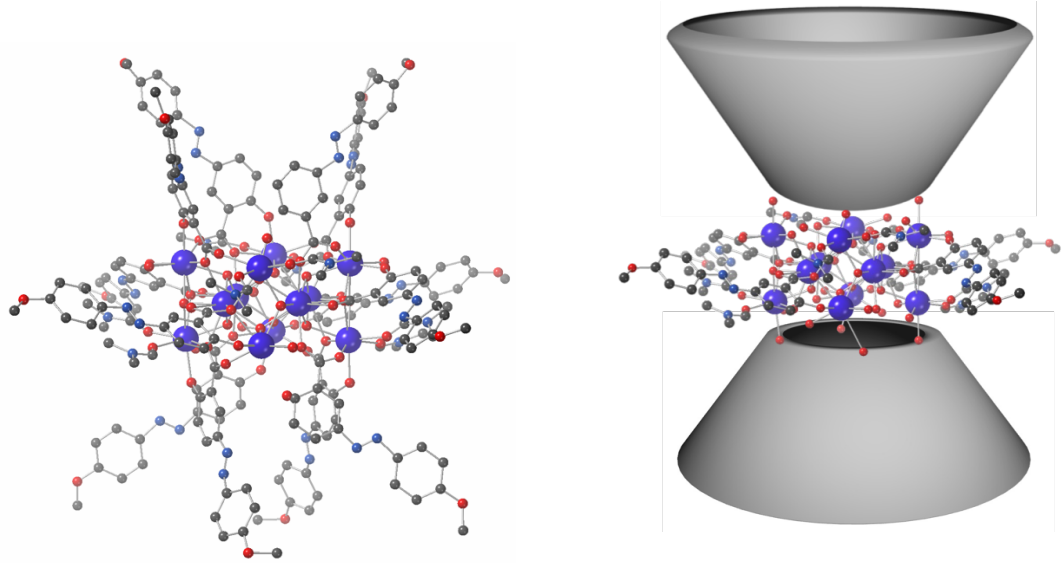

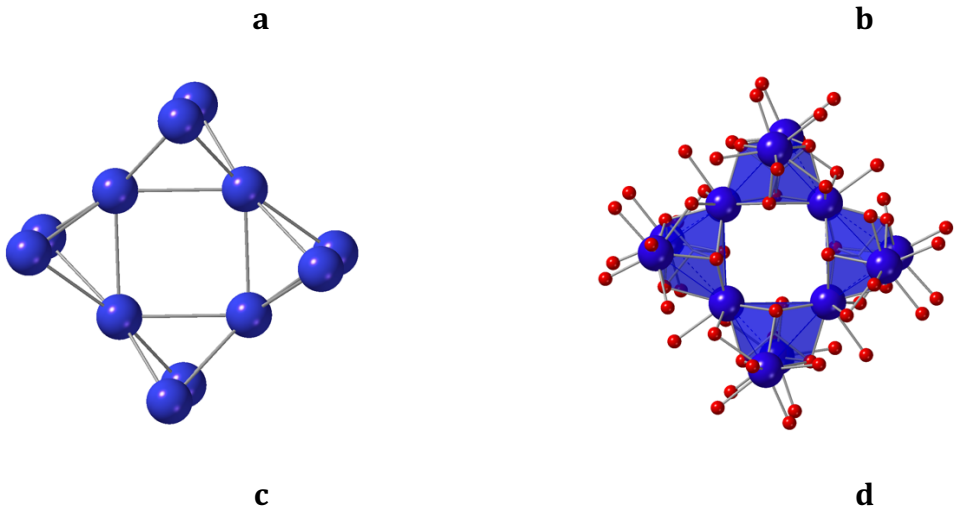

Figure 4. Side view of crystal structure of obtained **Dy_{12}-L2** (a) and schematic representation calix-shaped cavities each formed by four coordinated salicylic ligands; (b) disposed from upper and bottom sides of dodeconuclear cluster core; (c)&(d) Cubane geometry of metallic cluster core formed by the fusion of four tetrahedrons with the Dy-atoms in the vertices for obtained {Dy_{12}}-clusters

The shape of obtained dodeconuclear Dy_{12} clusters can be described as vertex-sharing metallocubanes, as shown in Figure 4 c and d, with the edges lengths equal to 6.147(6) Å, 6.249(6) Å, 4.155(7) Å for **Dy_{12}-L1**, 6.151(1) Å, 6.279(1) Å, 4.096(1) Å for **Dy_{12}-L2** and 6.210(2) Å, 6.201(2) Å, 4.050(1) Å for **Dy_{12}-L3**, and 6.181(1) Å, 6.320(2) Å 4.049(2) Å for **Dy_{12}-L3**. Some examples demonstrating the formation of similar metallic cores of type **A** (Figure 1) have been already encountered in the literature, together with the observed distances in accordance to what has been reported in the literature.[11,12,13]

As already mentioned, all salicylic derivatives **L1**-**L4** are found to be doubly deprotonated in the complexes, displaying two different coordination modes (bidentate or bis-monodentate) and bridging two metallic centers by O-atoms belonging to deprotonated

hydroxyl and carboxylic groups. Consequently, the coordination sphere around the Dy^{3+} cations are composed of either eight or nine O-atoms, presenting different geometries as analyzed using the SHAPE program.[35] The results are presented in Table S6. Since **Dy_{12}-L3** and **Dy_{12}-L4** adopt a lower symmetry structure, there are 6 nonequivalent Dy^{3+} cations (figure S15) which may be divided into two analogous A and B sets each composed of three metallic ions. The detailed analysis of distortion around the coordination spheres revealed that whereas the Dy^{3+} cations in **Dy_{12}-L1** and **Dy_{12}-L2** complexes adopt mostly Triangular dodecahedron (TDD-8, D*2d*), Square antiprism (SAPR-8, D*4d*) or muffin (MFF-9, C*s*) geometries characterized with rather small values of CShM distortion parameter, for **Dy_{12}-L3**, Dy^{3+} cations present different coordination sphere geometries like MFF-9, TDD-8, Johnson Bi-augmented trigonal prism J50 (JBTP-8, C*2v*) and Snub disphenoid J84 (JSD-8, D*2d*) characterized by more pronounced distortion. For **Dy_{12}-L4**, the coordination spheres appear relatively more symmetrical for those observed for **Dy_{12}-L1**, **Dy_{12}-L2** and **Dy_{12}-L3** (MFF-9, CSAPR-9, TDD-8 or BTPR-8 geometries, see SI).

Within the formed clusters **Dy_{12}-L2** and **Dy_{12}-L3**, intramolecular CH/π-bonding is observed. For **Dy_{12}-L2**, one of two DMF molecules coordinated to Dy-II cation (see SI, Table S6 and figure S15) interacts with the aryl moiety of salicylic ligand connected to Dy-III cation *via* one methyl group ($d_{CH...C6centroid}$ = 3.507 Å). Within the **Dy_{12}-L3** complex, there were found five from six independent DMF molecules which are involved in CH-π interaction *via* CH_3- or CH-formyl groups with aryl unit belonging to salicylic ligands connected to the same Dy-IIA (Dy-IIB) or Dy-IIIA (Dy-IIIB) cations with the CH…C6 centroid distances laying in the range of 3.241–3.677 Å. Due to the observed coordination pattern, short Dy-Dy distances are

observed in the 3.5340(16)- 3.5792(13) range for all the compounds. (see SI, Figure S15 and table S5).

The compounds present different crystal packing. In **Dy_{12}-L1** and **Dy_{12}-L2** the clusters are arranged in 3D molecular network displaying a *diamond-like* structure, as shown in Figure 5, due to the three-center CH-π interactions involving one CH_3 group of coordinated DMF, aromatic systems of salicylic moieties belonging to adjacent cluster molecules, for **Dy_{12}-L1** (Figure S16) ($d_{C96(DMF)...C6centroid}$ = 3.252 Å, $d_{C13...C6centroid}$ = 3.480 Å) and inclusion complex formation resulting from the insertion of one 4-OMePh-moiety into the calix-like cavity belonging to neighboring clusters with observed C16(OMe)…N6 distance equal to 3.181 Å, for **Dy_{12}-L2**. In addition, the cluster molecules of **Dy_{12}-L2** are also linked *via* CH-π bonding between CH_3 (DMF) group and aryl moiety of salicylic acid ($d_{C46...C18}$ = 3.285 Å). As a result, the distances between the cluster centers are found to be equal to 16.601 Å for **Dy_{12}-L1** and 18.194 Å for **Dy_{12}-L2**, which is in accordance with those observed for earlier reported familiar {Dy_{12}}-compound ($d_{\{Dy12\}...\{Dy12\}}$ = 17.044-17.828 Å).[12]

In contrast, the supramolecular architecture of **Dy_{12}-L3** in the crystalline phase is 2D grids leading to accessible channels, due to CH/π interactions, similar to those observed for **Dy_{12}-L2,** when the 4-nitrophenyl moiety is included into the calix-like cavity of adjacent cluster molecule leading to O (NO_2)… N distance equal to 2.91(2) Å both with π-π stacking involving the A and B azophenyl units of nitrophenyl substituents (see table S4). Each connecting node is composed of four stacked aromatic units belonging to four adjacent clusters ($d_{C6centroidA-C6centroidA}$ = 3.319 Å, dihedral angle 1.47^0, $d_{C6centroidA-C6centroidB}$ = 3.596, dihedral angle 6.54^0). Distances between the cluster centers are found to be equal to 17.18 Å, 21.02 Å and 21.64 Å along *a*, *b*, *c* axes, respectively. In **Dy_{12}-L4**, the clusters are stacked into the chains running

along *c* axe where the connection is ensured by CH-π interactions between included phenyl unit belonging to azophenyl substituent of one cluster molecule with the hydrophobic calix-like cavity of another ($d_{C10...N70}$ = 3.27(2) Å, $d_{C62...N10}$ = 3.40(2) Å, $d_{C84\ N19}$ = 3.44(3) Å, $d_{C86...N1}$ = 3.46(1) Å) (see Figure S3). The interconnection between the chains is supported by relatively weaker CH-π bonding involving C-atom belonging to coordinated DMF molecule and azophenyl moiety ($d_{C27...C6centroid}$ = 3.592 Å) as well as azophenyl moieties ($d_{C104...C6centroid}$ = 3.675 Å) (see Figure S16): this leads to an overall structure presenting hexagonal cavities. The cluster molecules belonging to adjacent chains display the angular orientation with 84.93^{O} between the axis passing through the center of their calix-like cavities.

It worth noting that whereas the 3D diamond-like architectures of **Dy_{12}-L1** and **Dy_{12}-L2** (Figure 5) present porous structures with the accessible voids volume equal to 2895 Å^{3}and 16878 Å^3 per unit cell (11.4% and 46.1%), respectively, according to *PLATON*.[36] The turning "on" the strong π-stacking interaction induced tight crystal packing in **Dy_{12}-L3**, afford a decreasing porosity and resulted in 1152 Å^3 of voids volume (15.8%). Surprisingly, the hexagonal self-assembly of clusters in **Dy_{12}-L4** produced 3D CH/π bonded molecular network containing large hexagonal pores of *ca.* 18 Å along *c* axe in the crystalline phase with accessible voids volume of 21389 Å^3 per unit cell (32.4 %) (Figures 5 and S17).

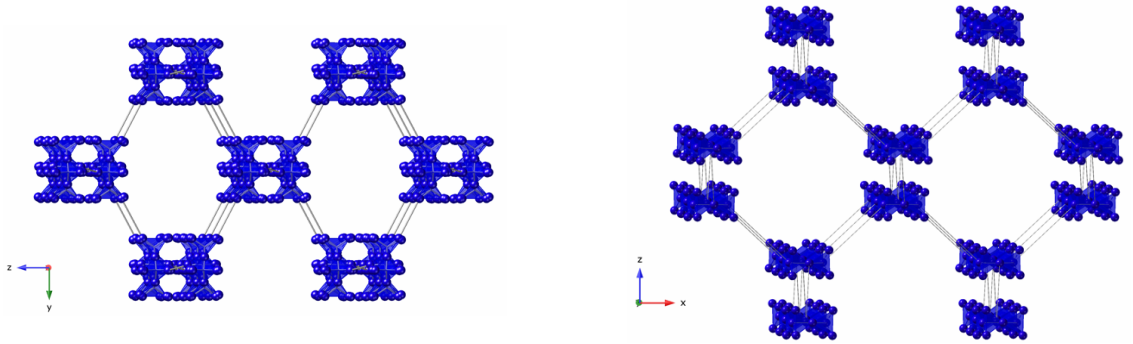

a **b**

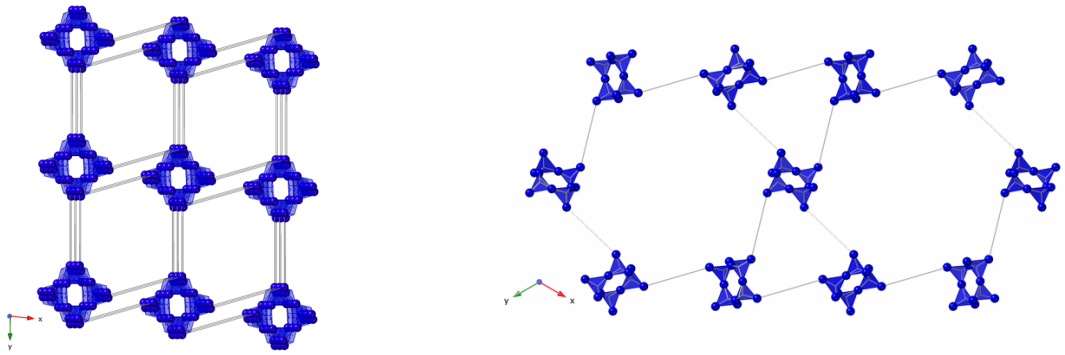

c **d**

Figure 5. For **Dy12-L1** (a), **Dy_{12}-L2** (b), **Dy_{12}-L3** (c) and **Dy_{12}-L4** (d), schematic representation of 3D CH/π molecular network connectivity pattern between the [Dy_{12}]-metallocubanes. C-,H-,N-,O- atoms are omitted for clarity. Dy^{3+} atoms are presented as blue spheres.

In **Dy_{12}-L1**-**Dy_{12}-L4** and as already mentioned, the interstices between the cluster's species are filled with solvent molecules, and they were not all refined.

XRPD measurements

The XRPD patterns are presented in Figures S18. For **Dy_{12}-L1**-**Dy_{12}-L4**, the main diffraction peaks are present, attesting the presence of the crystalline compound in the polycrystalline powder, but the slight shifts and broadening of the peaks on the XRPD pattern are attesting the slight desolvation of the compounds, as frequently observed for huge molecules of such high nuclearity clusters in the solid state, when exposed to the air.

Thermogravimetric analysis (TGA)

The TGA measurements for microcrystalline powder of **Dy_{12}-L1**-**Dy_{12}-L4** (Figure S20) show that the mass loss begins at ambient conditions. This is consistent with the presence of crystallization solvents in the crystal and changes in PXRD described above

during exposure to the air. Unfortunately, from the obtained data, the amount and nature of solvents could not be refined and is different from the one obtained by EA, due to a large amount of solvent release when exposed to the air.

Magnetic properties of Dy_{12}-L1, Dy_{12}-L2, Dy_{12}-L3, and the UV-light-irradiated Dy_{12}-L1

The magnetic properties have been investigated for three compounds **Dy_{12}-L1**, **Dy_{12}-L2**, and **Dy_{12}-L3**, in order to study the electron donor (R = CH_3, OMe) or electron withdrawing groups (NO_2) influence on their magnetic relaxation behavior.

The room-temperature $\chi_M T$ product values for **Dy_{12}-L1**, **Dy_{12}-L2**, and **Dy_{12}-L3** (178 $cm^3mol^{-1}K$ for **Dy_{12}-L1** and **Dy_{12}-L3**, and 172 $cm^3mol^{-1}K$ for **Dy_{12}-L2**) are in accordance with those expected for 12 non-interacting Dy^{3+} ions (Figure 6). Upon cooling from 300 to ca. 70 K, the $\chi_M T$ products slowly decrease in all compounds which can be mainly ascribed to the single-ion properties of Dy^{3+} ions, that is the cooling-induced depopulation of the higher-lying m_J states within the ground multiplets. At lower temperatures, the decrease of the $\chi_M T$ value is stronger, down to 135–150 $cm^3mol^{-1}K$. Such a decrease can be correlated with the appearance of magnetic exchange coupling of the antiferromagnetic character within the obtained multimetallic coordination clusters. The related magnetic interactions are relatively weak as illustrated by the large remaining $\chi_M T$ values at 1.8 K, as well as by the monotonous increase of the molar magnetization upon the increasing field at 1.8 K (Figure 6). It is in accordance with what was already observed for related Dy_{12} clusters.[12] The related magnetization of ca. 60 μ_B at 60 kOe gives ca. 5 μ_B per each Dy(III) center which is a typical

value even for the perfectly isolated complexes of this metal ion, confirming the weak magnetic exchange within the cluster core.

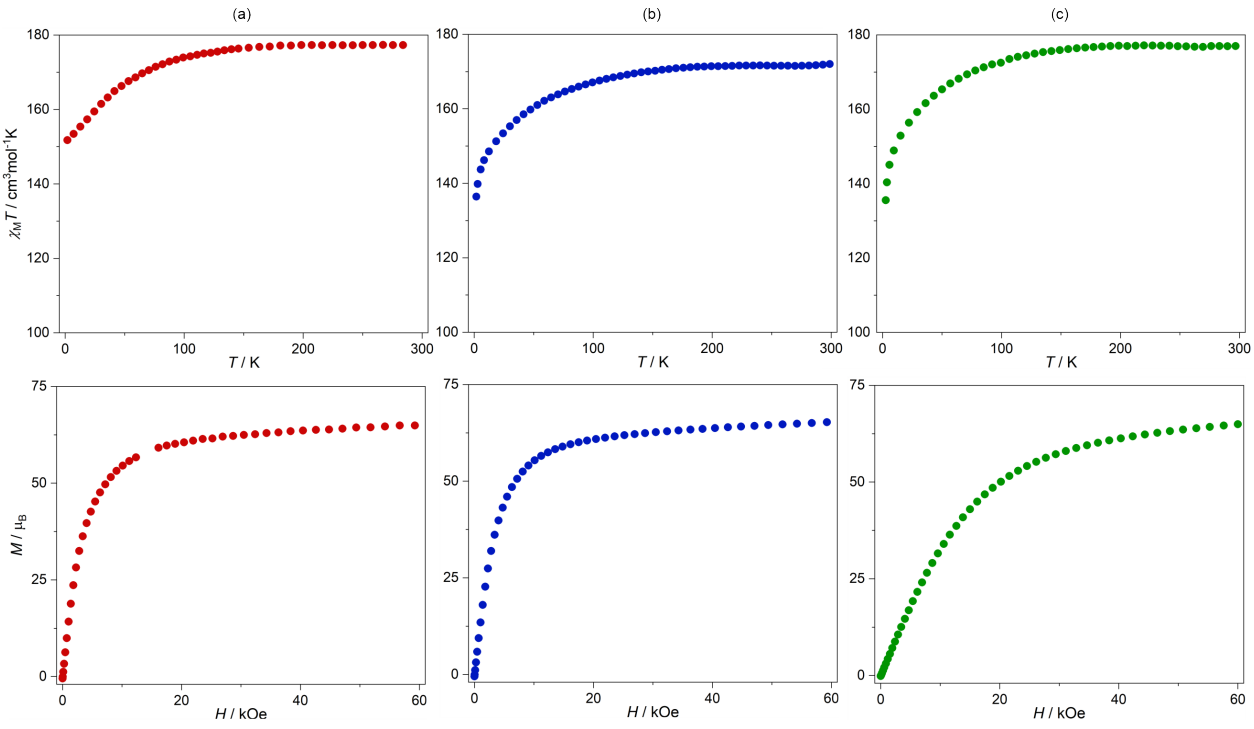

Figure 6. Direct-current (*dc*) magnetic properties of **Dy$_{12}$-L1** (a), **Dy$_{12}$-L2** (b), and **Dy$_{12}$-L3** (c), including the temperature dependences of the $\chi_M T$ product at H_{dc} = 1 kOe (top part) and the field dependences of molar magnetization at T = 1.8 K (bottom part).

Due to the presence of Dy(III) centers embedded in the coordination clusters further isolated from the neighboring ones, the obtained compounds were promising candidates for the observation of SMM behavior. To examine this, the alternate-current (*ac*) magnetic measurements were performed for **Dy$_{12}$-L1**, **Dy$_{12}$-L2**, and **Dy$_{12}$-L3** (Figures 7 and S21-S23). All these compounds exhibit the slow relaxation of magnetization under the zero *dc* magnetic field below 7 K as visualized by the related *ac* magnetic characteristics, e.g., the frequency

dependences of the out-of-phase magnetic susceptibility showing distinct maxima in the accessible 1–1000 Hz range. This indicates SMM behavior. It gradually disappears under the increased *dc* magnetic field which is a typical effect for the multimetallic-cluster-based SMMs. The sets of zero-*dc*-field *ac* magnetic data for all three compounds were analyzed using the generalized Debye model providing the temperature-dependent magnetic relaxation times (Figure 7, bottom part). For **Dy_{12}-L1** and **Dy_{12}-L2**, a single relaxation process was found. In **Dy_{12}-L3**, two relaxation processes were detected which could be explained by the presence of two slightly structurally different clusters in the crystal lattice, related, e.g., to the structural disorder of the bulky organic ligands. Thus, for the **Dy_{12}-L3**, two relaxation times were determined. The temperature dependences of the relaxation times, presented in the Arrhenius-type form of $\ln(\tau)$ versus T^{-1}, were found to be closely linear as characteristics of the Orbach relaxation process usually observed for the cluster-based SMMs. For both relaxation pathways in **Dy_{12}-L3**, the linearity of the $\ln(\tau)$ versus T^{-1} is almost perfect. Therefore, for this compound, the sole contribution of the Orbach relaxation, depicted by the equation: $\tau^{-1}(T) = \tau_0^{-1}\exp(-U_{eff}/T)$, could be employed. The best-fit curves provide the following set of parameters: U_{eff} = 2.39(2) K with $\tau_0 = 3.79(3)\cdot10^{-3}$ s for slower relaxation and U_{eff} = 2.94(8) K with $\tau_0 = 1.33(4)\cdot10^{-4}$ s for faster relaxation. The energy barriers are relatively small indicating the moderate SMM behavior related to the only weakly magnetically anisotropic Dy(III) centers embedded in the cluster core.[51] For **Dy_{12}-L1** and **Dy_{12}-L2**, the discrepancy from the linearity of the $\ln(\tau)$ versus T^{-1} curves was too large to solely employ the Orbach relaxation. Therefore, the Raman process was added into consideration; thus, the equation of $\tau^{-1}(T) = \tau_0^{-1}\exp(-U_{eff}/T) + B_{Raman}T^n$, was used. The best-fit parameters are U_{eff} = 4.68(4) K, $\tau_0 = 2.37(5)\cdot10^{-4}$ s, B_{Raman} = 0.15(5) $s^{-1}K^{-n}$, and n = 4.88(17)

for **Dy$_{12}$-L1**, and U_{eff} = 4.65(9) K, τ_0 = 2.22(8)·10^{-4} s, B_{Raman} = 7.6(3)·10^{-4} s^{-1}K^{-n}, and n = 7.3(9) for **Dy$_{12}$-L2**. The energy barriers are visibly enhanced when compared with **Dy$_{12}$-L3**, indicating the role of the ligand substituent in the packing and also in the modulation of the magnetic anisotropy of incorporated Dy(III) centers. The Raman process plays generally a minor role; however, it becomes significant at relatively higher temperatures, probably in the region where the magnetic exchange within the clusters is weakened.

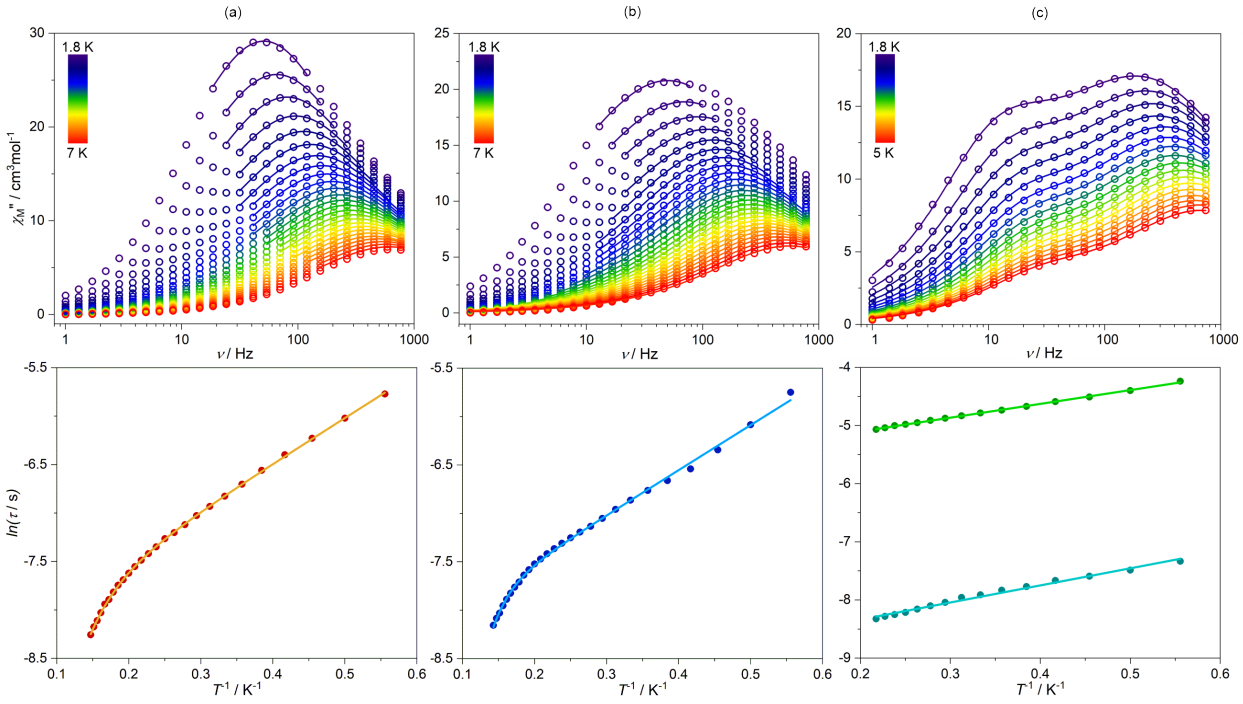

Figure 7. Representative alternate-current (*ac*) magnetic characteristics of the zero-*dc*-field slow magnetic relaxation effect in **Dy$_{12}$-L1** (a), **Dy$_{12}$-L2** (b), and **Dy$_{12}$-L3** (c), including the frequency dependences of the out-of-phase magnetic susceptibility under the variable, indicated temperatures (top part, H_{ac} = 3 Oe) and the temperature dependences of the resulting magnetic relaxation times (bottom part). In the top part, the colored points represent the experimental data while the solid lines depict the best fits obtained following a generalized Debye model. In the bottom part, the colored points represent the

experimental data while the solid lines depict the best fit to the combined contributions from the Orbach and Raman processes (see the text for details). The full sets of *ac* magnetic characteristics for all three compounds are shown in Figures S21-S23.

Because of the presence of the photoswitchable azobenzene ligands, one compound (**Dy_{12}-L1**) was irradiated (12-hour-lasting irradiation of the powder sample by the directly attached 5W 365 nm light source, see experimental part) and the *ac* magnetic data after the irradiation were recorded (Figures 8 and S24). The slow magnetic relaxation appears to be slowed down as visualized by the shift of the respective maxima of the out-of-phase magnetic susceptibility towards higher frequencies when compared with the sample before irradiation (see Figures 7a and 8). The precise analysis of the *ac* data for the UV-light-irradiated sample was performed using the generalized Debye model. The resulting temperature dependence of the magnetic relaxation times was analyzed in the analogous way as described above for the sample of **Dy_{12}-L1** before irradiation. The best-fit parameters are U_{eff} = 4.18(7) K, τ_0 = 1.22(5)·10^{-4} s, B_{Raman} = 4.1(2)·10^{-2} $s^{-1}K^{-n}$, and n = 5.8(16). The effective energy barrier is decreased when compared with the sample before irradiation indicating that the structural modification, presumably related to the partial *trans–cis* photoisomerization of the organic ligands, leads to the weakening of the SMM effect. Unfortunately, due to the loss of crystallinity after the irradiation process, the structure could not be refined.

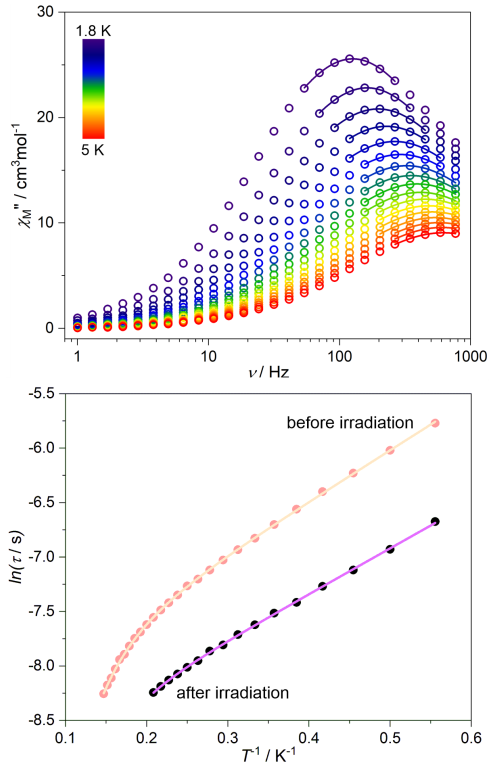

Figure 8. The representative *ac* magnetic characteristics of **Dy_{12}-L1** after UV light irradiation, including the frequency dependences of the out-of-phase magnetic susceptibility under the variable indicated temperatures (top part, H_{ac} = 3 Oe) and the temperature dependences of the resulting magnetic relaxation times (bottom part). In the top part, the colored points represent the experimental data while the solid lines depict the best fits obtained following a generalized Debye model. In the bottom part, the colored points represent the experimental data while the solid lines depict the best fit to the combined contributions from the Orbach and Raman processes (see the text for details). The full sets of *ac* magnetic characteristics are shown in Figure S24. In the bottom part, the magnetic relaxation curve for the **Dy_{12}-L1** sample before irradiation (Figure 7a) was presented for comparison.

CONCLUSIONS

The use of salicylic ligands (**L1**-**L4**) with an azobenzene scaffold, appended with different chemical groups, allows to obtain a series of four different dodecanuclear Dy^{3+} clusters (**Dy_{12}-L1**-**Dy_{12}-L4**). The clusters, four vertex-sharing heterocubanes or tetrahedra (Type **A**) present a metallic core, bridged by 8 hydroxyl moieties, and capped by 6 ligands. Some Coordinating DMF or water molecules are also present, and within the crystal, some solvent molecules have also been refined. Depending on the nature of the appended groups, different arrangement for the compounds have been observed in the crystal, leading to compounds presenting a high porosity, revealed by the supramolecular arrangement involving weak CH/π interactions. The study of magnetic properties for **Dy_{12}-L1**, **Dy_{12}-L2** and **Dy_{12}-L3** clusters revealed that all of them exhibit a SMM magnetic behavior at low temperature. It was shown that the ligands bearing donor groups (CH_3 and OMe) in *para* position with respect the azo group, display similar magnetic relaxation as well as the crystalline assembly (3D diamond like structures). At the same time, the replacement of donor electron group by withdrawing NO_2 group resulted in the slightly decrease of the anisotropy barrier of the **Dy_{12}-L3** clusters displaying also an absolutely different supramolecular organization in the crystalline phase (2D π-stacked sheets). For this reason, there is no possibility to unambiguously conclude which factor (the presence of the electron donor/withdrawing group or the packing) play the crucial role in the magnetic behavior of these {Dy_{12}}-systems. The attempt to achieve the photo-control over the magnetic properties due to the presence of photoswitchable azophenyl moieties was performed upon the UV-irradiation of **Dy_{12}-L1** cluster leading to decreasing of magnetic relaxation life time. To the best of our knowledge, this is the first example of lanthanide based solid-state complex, containing azo-groups,

showing the SMM behavior depended on the UV-irradiation. Further investigation will be continued in order to shed light on the mechanism of the magnetic relaxation of the lanthanide SMMs upon the light-irradiation.

ASSOCIATED CONTENT

Supporting Information. Characterization of the **L4**-**L4** ligands; for **Dy_{12}-L1**-**Dy_{12}-L4**, Crystallographic data for the clusters, pictures of the crystals, main bonds, distances and angles, full SHAPE analysis representation of the asymmetric units and visualization of the supramolecular interactions, XRPD diagrams, IR-spectra and TGA/DSC traces. For **Dy_{12}-L1**-**Dy_{12}-L3**, in-phase and out-of-phase susceptibility and for irradiated **Dy_{12}-L1**, magnetic measurements.

The following files are available free of charge.

AUTHOR INFORMATION

Corresponding Author

ferlay@unistra.fr

Author Contributions

All authors have given approval to the final version of the manuscript.

Funding Sources

Russian Science Foundation (Project № 22-73-10139).

Notes

The contribution from Jakub J. Zakrzewski and Dr. Szymon Chorazy (Jagiellonian University, Krakow, Poland) to this work was realized in 2021.

ACKNOWLEDGMENT

This work was supported by the University of Strasbourg, a Doctoral Mechnikov scholarship from French Embassy in the Russian Federation (I. V. K.), the Fondation Jean-Marie Lehn, the CNRS, the Russian Science Foundation (Project № 22-73-10139 to A. S. O.).

The authors are grateful to Kurchatov Complex For Synchrotron And Neutron Investigations for performing of X-ray diffraction- on single crystals (Dorovatovskii P.V.), to Spectral-Analytical Center of FRC Kazan Scientific Center of RAS for their help and support in TGA (Dr. Ayrat R. Khamatgalimov) XRPD analysis (Dr. Alina F. Saifina) and IR studies. The Russian authors warmly thank Dr. Zaliya V. Akhmetzyanova and Prof. Igor S. Antipin for their help and support in the synthesis of the prepared coordination compounds.

REFERENCES

1 Dechambenoit, P.; Long, J. R. Microporous magnets *Chem. Soc. Rev*., **2011**, *40*, 3249-3265

2 Espallargas, G. M.; Coronado, E. Magnetic functionalities in MOFs: from the framework to the pore *Chem. Soc. Rev*., **2018**, *47*, 533-557.

3 Thorarinsdottir, A. E.; Harris, T. D. Metal–Organic Framework Magnets, *Chem. Rev.* **2020**, **120**, 8716–8789.

4 Aldoshin, S. M.; Korchagin, D. V.; Palii, A. V.; Tsukerblat, B. S. Some new trends in the design of single molecule magnets *Pure Appl. Chem*., **2017**, *89*, 1119-1143.

5 a) Sessoli, R.; Powell, A. K. Strategies towards single molecule magnets based on lanthanide ions. *Coord. Chem. Rev*. **2009**, *253*, 2328-2341.

b) Woodruff, D. N.; Winpenny, R. E. P.; Layfield, R. A. Lanthanide Single-Molecule Magnets *Chem. Rev*. **2013**, *113*, 5110-5148.

c) Craig, G. A.; Murrie, M. 3d single-ion magnets. *Chem. Soc. Rev*. **2015**, *44*, 2135-2147.

d) Feng, M.; Tong, M.-L. Single Ion Magnets from 3d to 5f: Developments and Strategies. *Chem. Eur. J*. **2018**, *24*, 7574-7594.

6 Rinehart, J.; Long, J. Exploiting single-ion anisotropy in the design of f-element single-molecule magnets, *Chem. Sci*., **2011**, *2*, 2078-2085.

7 Zabala-Lekuona, A.; Seco, J. M.; Colacio, E. Single-Molecule Magnets: From Mn_{12}- to dysprosium metallocenes, a travel in time *Coord. Chem. Rev*., **2021**, *441*, 213984.

8 Zheng, X-Y.; Xie, J.; Kong, X-J.; Long, L-S.; Zheng, L-S. Recent advances in the assembly of high-nuclearity lanthanide clusters *Coord. Chem. Rev*., **2019**, *378*, 222-236.

9 Zheng, X-Y.; Kong, X-J; Zheng, X-Y.; Long, L-S; Zheng L-S. High-Nuclearity Lanthanide-Containing Clusters as Potential Molecular Magnetic Coolers *Acc. Chem. Res*., **2018**, *51*, 517-525.

10 Peng, J-B.; Kong, X-J;. Zhang, Q-C.; Orendáč, M.; Prokleška, J;. Ren, Y-P.; Long, L-S.; Zheng, Z.; Zheng, L-S. Beauty, Symmetry, and Magnetocaloric Effect-Four-Shell Keplerates with 104 Lanthanide Atoms *J. Am. Chem. Soc*. **2014**, *136*, 17938-17941.

11 Wang, R.; Selby, H. D.; Liu, H.; Carducci, M. D.; Jin, T.; Zheng, Z.; Anthis, J. W.; Staples, R. J. Halide-templated assembly of polynuclear Lanthanide-hydroxo complexes *Inorg. Chem*. **2002**, *41*, 278-286.

12 Dinca, A. S.; Mindru, A.; Dragancea, D.; Tiseanu, C.; Shova, S.; Cornia, S.; Carrella, L. M.; Rentschler, E.; Affronte, M.; Andruh M. Aggregation of $[Ln^{III}_{12}]$ clusters by the dianion of 3-formylsalicylic acid. Synthesis, crystal structures, magnetic and luminescence properties *Dalton Trans*. **2019**, *48*, 1700-1708.

13 Miao, Y.-L.; Liu, J.-L.; Leng, J.-D.; Lin, Z.-J.; Tong, M.-L. Chloride templated formation of $\{Dy_{12}(OH)_{16}\}^{20+}$ cluster core incorporating 1,10-phenanthroline-2,9-dicarboxylate *CrystEngComm*, **2011**, *13*, 3345-3348.

14 Zhao, L.; Xue, S.; Tang, J. A Dodecanuclear Dysprosium Wheel Assembled by Six Vertex-Sharing Dy3 Triangles Exhibiting Slow Magnetic Relaxation *Inorg. Chem*. **2012**, *51*, 5994-5996.

15 Banerjee, S.; Kumar, G. A.; Riman, R. E.; Emge, T. J.; Brennan, J. G. Oxoclusters of the Lanthanides Begin to Resemble Solid-State Materials at Very Small Cluster Sizes: Structure and NIR Emission from Nd(III) *J. Am. Chem. Soc*. **2007**, *129*, 5926-5931.

16 Li, Y-M.; Kuang, W-W.; Zhu, L-L.; Xu, Y.; Yang, P-P. Two Discrete Ln12 Shelf-Shaped Clusters: Magnetic Studies Reveal a Significant Cryogenic Magnetocaloric Effect and Slow Magnetic Relaxation *Eur. J. Inorg. Chem*. **2016**, 4996-5003

17 D'Alessio, D.; Sobolev, A. N.; Skelton, B. W.; Fuller, R. O.; Woodward, R. C.; Lengkeek, N. A.; Fraser, B. H.; Massi, M.; Ogden, M. I. Lanthanoid "Bottlebrush" Clusters: Remarkably Elongated Metal–Oxo Core Structures with Controllable Lengths *J. Am. Chem. Soc.* **2014**, *136*, 15122-15125.

18 Luo, Z-R.; Zou, H-H.; Chen, Z-L.; Li, B.; Wang, K.; Liang, F-P. Triethylamine-templated nanocalix Ln12 clusters of diacylhydrazone: crystal structures and magnetic properties *Dalton Trans*., **2019**, *48*, 17414-17421.

19 Bandara, H. M. D.; Burdette, S. C. Photoisomerization in Different Classes of Azobenzene. *Chem. Soc. Rev*., **2012**, *41*, 1809-1825.

20 Tylkowski, B.; Trojanowska, A;. Marturano, V.; Nowak, M.; Marciniak, L.; Giamberini, M.; Ambrogie, V.; Cerruti, P. Power of light–Functional complexes based on azobenzene molecules *Coord. Chem. Rev*. **2017**, *351*, 205-217.

21 Akitsu, T.; Nishijo, J. The first observation of photoinduced tuning of AC magnetization for organic–inorganic hybrid materials composed of Mn12-acetate and azobenzene *J. Magn. Magn. Mater*., **2007**, *315*, 95-100.

22 Akitsu, T.; Ishioka, C;. Itoh, T. Polarized light spectroscopy of azobenzene or disperse red 1 with Mn12 single-molecule magnets in PMMA film hybrid materials Cent. *Eur. J. Chem*. **2009**, *7*, 690-696.

23 George, S. M.; Kim, J. Synthesis and photoinduced magnetic properties of a Mn_{12} single molecule magnet by the cis-trans isomerism of azobenzene, *Bull. Korean Chem. Soc*., **2009**, *30*, 1143-1146.

24 Prasad, T. K; Poneti, G.; Sorace, L.; Rodriguez-Douton, M. J.; Barra, A-L.; Neugebauer, P.; Costantino, L.; Sessoli, R.; Cornia, A. Magnetic and optical bistability in tetrairon(III) single molecule magnets functionalized with azobenzene groups *Dalton Trans*. **2012**, *41*, 8368-8378.

25 Nakamura, K;. Kondo, M.; Krishnan, C. G.; Takizawa, S.; Sasai H. Azopyridine-based chiral oxazolines with rare-earth metals for photoswitchable catalysis *Chem. Commun*. **2021**, *57*, 7414-7417.

26 Dolomanov, O. V.; Bourhis, L. J.; Gildea, R.J.; Howard, J. A. K.; Puschmann, H. J. OLEX2: A Complete Structure Solution, Refinement and Analysis Program. *Appl. Cryst.* **2009**, *42*, 339-341.

27 Sheldrick, G. M. SHELXT: Integrating space group determination and structure solution. *Acta Crystallogr.* **2015**, *71*, 3-8

28 Sheldrick, G. M. A Short History of SHELX. *Acta Crystallogr*. **2007**, *64*, 112-122.

29 Lazarenko, V. A.; Dorovatovskii, P. V.; Zubavichus, Y. V.; Burlov, A. S.; Koshchienko, Y. V.; Vlasenko, V. G.; Khrustalev, V. N. High-throughput small-molecule crystallography at the 'Belok' beamline of the Kurchatov synchrotron radiation source: Transition metal complexes with azomethine ligands as a case study. *Crystals*, **2017**, *7*, 11, 325.

30 Svetogorov, R. D.; Dorovatovskii, P. V.; Lazarenko, V. A. Belok/XSA diffraction beamline for studying crystalline samples at Kurchatov Synchrotron Radiation Source. *Crystal Research and Technology*, **2020**. *55*, 5, 1900184.

31 Kabsch, W. XDS. *Acta Crystallogr*. **2010**, D66, 125-132.

32 Guzei, I. A. An idealized molecular geometry library for refinement of poorly behaved molecular fragments with constraints. *J. Appl. Crystallogr.* **2014**, *47*, 806-809.

33 Harveer, K; Jasmeen, S.Synthesis, characterization and radical scavenging activity of aromatic amine conjugates of 5-aminosalicylic acid *Bull. Chem. Soc. Ethiop*., **2014**, *28*, 475-480.

34 Zhang, X.; Zhong, F.; Liu, J.; Xu, H.; Gao, J.; Xu, S.; A New Three-dimensional Metal-organic Framework based on Dinuclear Rare Earth Cluster and Olsalazine *Z. Anorg. Allg. Chem*., **2019**, *645*, 1267-1270.

35 Llunell, M.; Casanova, D.; Cirera, J.; Bofill, J. M.; Alemany, P.; Alvarez, S.; Pinsky, M.; Avnir, D. SHAPE, version 2.3, University of Barcelona, Barcelona, Spain, and Hebrew University of Jerusalem, Jerusalem, Israel, **2013**.

36 Spek, A. L. PLATON, A Multipurpose Crystallographic Tool; Utrecht University: Utrecht, The Netherlands, **2001**

TOC

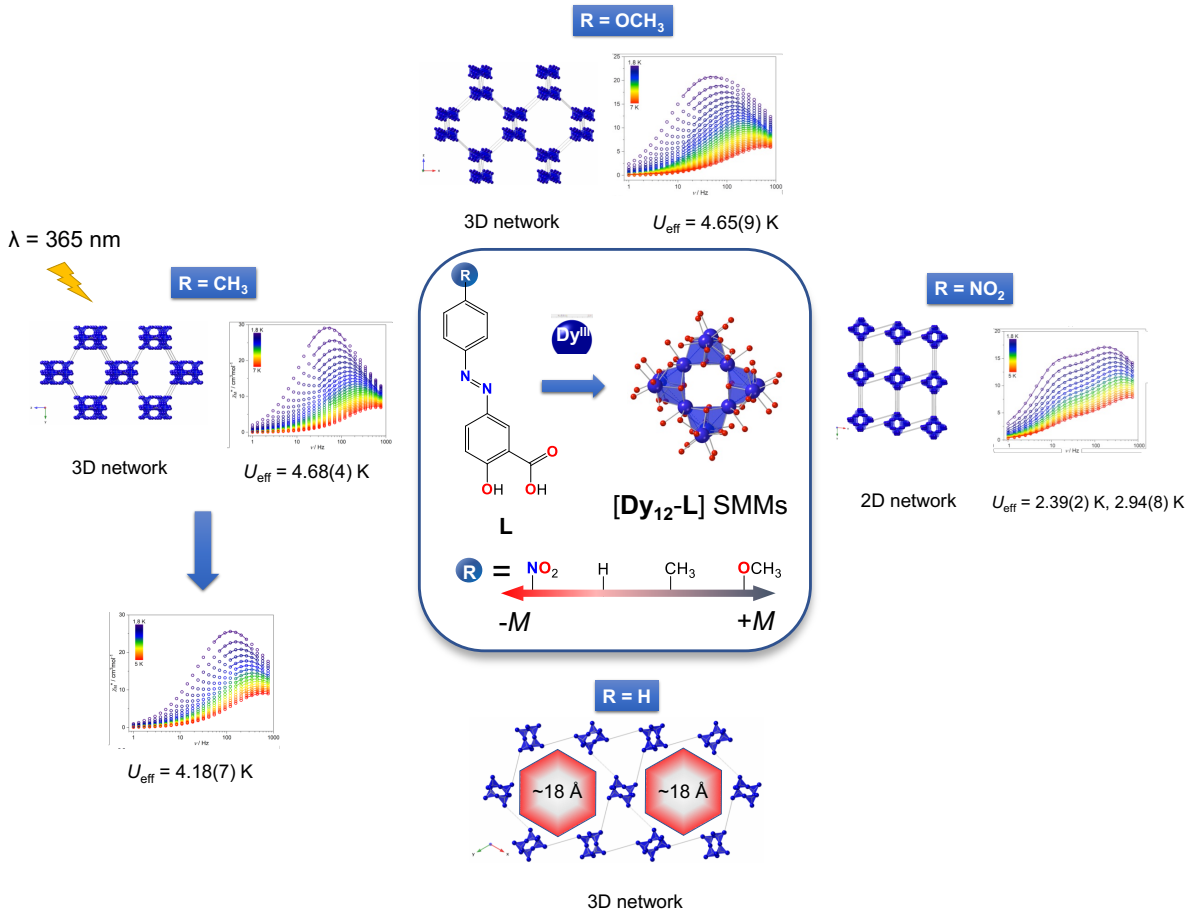

A series of four new Dy_{12} dodecanuclear clusters based on azobenzene derivative ligands of salicylic acid has been synthesized and characterized from a structural point of view. Three of these clusters display a SMM magnetic behavior, their short lifetimes have been measured, and, for one compound, preliminarily data concerning the irradiation of the solid-state powder, have been reported.